

Modeling study of scattering and absorption properties of tar-ball aggregates

LI LIU¹ AND MICHAEL I. MISHCHENKO^{2,*} 

¹Columbia University and NASA Goddard Institute for Space Studies, 2880 Broadway, New York, New York 10025, USA

²NASA Goddard Institute for Space Studies, 2880 Broadway, New York, New York 10025, USA

*Corresponding author: michael.i.mishchenko@nasa.gov

Received 29 August 2019; revised 8 October 2019; accepted 8 October 2019; posted 9 October 2019 (Doc. ID 376732); published 1 November 2019

Atmospheric tar balls (TBs) form an important class of atmospheric brown carbon (BrC) particulates. The morphology of the individual TBs is typically described as amorphous and nearly spherical. However, several studies reported observations of TBs aggregated with other aerosols or agglomerations consisting of up to tens of individual TBs. We use the superposition *T*-matrix method to compute the scattering matrix elements and optical cross sections for a variety of TB aggregates, each of which is composed of a number of monomers whose sizes follow a lognormal distribution. The results for a TB aggregate can differ fundamentally from those calculated for two simplified models commonly used in climate modeling; viz., the external mixture of TBs and the respective volume-equivalent sphere model. Clustering of individual TBs into an aggregate can either enhance or weaken absorption depending on the wavelength, the monomer size, and how absorptive the BrC material is. In the case of strongly absorptive BrC, aggregation results in enhanced absorption only at 1064 nm, while at 355 and 532 nm TB aggregates become less effective absorbers relative to the corresponding external mixtures. The effect of aggregation is always to increase the single-scattering albedo and asymmetry parameter, sometimes more than tenfold. The significant scattering-matrix differences between a TB aggregate, the “equivalent” external mixture, and the volume-equivalent sphere model demonstrate the failure of the conventional Lorenz–Mie theory to represent the scattering properties of morphologically complex BrC aerosols. We show that TB aggregates can help explain exceptionally strong and spectrally dependent lidar depolarization ratios reported in several recent studies. ©

2019 Optical Society of America

<https://doi.org/10.1364/AO.58.008648>

1. INTRODUCTION

Atmospheric tar balls (TBs) are a specific type of carbonaceous aerosols commonly formed during smoldering combustion of biomass materials [1–7]. Abundant in slightly aged biomass burning smoke and considered to be a member of brown carbon (BrC) family, TBs play a significant but highly uncertain role in Earth’s radiation budget [8].

Unlike black carbon particles, which possess a distinctive agglomerate morphology and are primarily released by high temperature combustion, individual atmospheric TBs have been widely described as being amorphous and spherical [1,3], and are often observed as being externally mixed with other biomass burning particles. However, there are numerous studies that report observations of TBs aggregated with other aerosols, or agglomeration of TBs into clusters of up to tens of individual TBs. In the Yosemite Aerosol Characterization Study in the summer of 2002 [2], small clusters of a few TBs were found very common, while larger clusters consisting of tens of individual TBs were also evident. Deboudt *et al.* [9] pointed out that

TBs or soot particles in their study could coagulate with dust particles to form carbonaceous aggregates at the surface of dust particles. In the study by Tóth *et al.* [10], atmospheric TBs were present as both individual particles and aggregates (Fig. 1). The laboratory study by Chakrabarty *et al.* [5] revealed that the two basic morphologies of TB aerosols were either individual spheres or agglomerates. Moreover, they stressed that a significant fraction (~60%) of the analyzed particles were agglomerates of TB spheres. Giroto *et al.* [8] reported observations of a significant fraction of TB aggregates from samples collected in a plume of the Whitewater–Baldy Complex fire in New Mexico. Most recently, agglomerated TBs have been observed in some transmission electron microscopy (TEM) images of biomass burning particulates from northwestern U.S. wild fires [11].

Different from black carbon aerosols whose primary particle sizes are small and narrowly distributed (e.g., [12,13]), the individual TB spheres are much bigger and span a much wider size range. For example, according to [3], the diameters of TBs are typically between 30 and 500 nm. Giroto *et al.* [8] found that

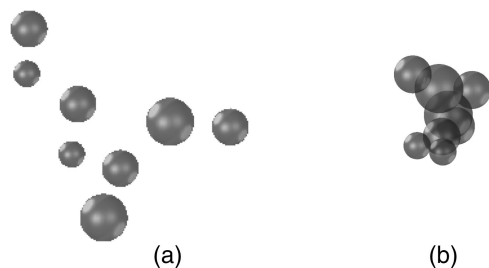


Fig. 1. Externally mixed (a) and aggregated (b) tar balls.

the diameters of the monomers in the TB aggregates fell between 62 and 458 nm. Bhandari *et al.* [6] observed that TBs usually have diameters between ~ 100 and 300 nm. On the other hand, black carbon tends to exist in the form of branching aggregates containing from fewer than 10 to thousands of spheres, each of which is 20 to 60 nm in diameter [12]. According to [13], the mean spherical monomer size in diameter ranges from 27 to 44 nm, and monomer cluster aggregation is dominant at the beginning of the coagulation process, resulting in a compact cluster. Later the cluster can become more branched out when aggregation is led by cluster–cluster agglomeration. There is a general consensus that aggregation of tiny highly absorptive black carbon spherules can result in a significant enhancement of absorption relative to that computed for an idealized external mixture of spherically shaped aerosols using the Lorenz–Mie theory [14–16]. Given that the sizes of the individual TBs are much larger and are widely distributed, and there is a significant spread in the reported values of the imaginary part of the BrC refractive index, the potential effects of aggregation on the optical properties of TB aggregates may be different from those for black-carbon aerosols.

To the best of our knowledge, Bhandari *et al.* [6] is the first systematic modeling study of the optical properties and radiative forcing of fractal-like TB aggregates resulting from biomass burning. Their numerical calculations using the numerically exact superposition T -matrix method (STMM) [17–19] showed that the optical properties of TB aggregates are different from those of the individual TBs and are not always well approximated by Lorenz–Mie calculations. Their findings highlight the necessity to account for the aggregation of TBs in global circulation models.

Building on the study by Bhandari *et al.* [6], we apply the same computer solver of the Maxwell equations for the calculation of the radiative properties of TB aggregates. However, the scope of our study is expanded to include polarization properties like the Stokes scattering matrix and the backscattering linear depolarization ratio (LDR), which are particularly useful in

remote-sensing studies of biomass burning aerosols. In addition, unlike in [6], we assume that the monomers in TB aggregates are polydisperse and follow a lognormal size distribution, as observed by Girotto *et al.* [8]. Moreover, for the same number of individual TB spheres of various sizes, their geometrical configurations to form a big aggregate are countless. Our results account for the effect of primary particle configurations on the radiative properties of TB aggregates by taking an ensemble average over 10 different aggregates with diverse morphologies formed by the same primary TB spheres.

2. TAR BALL AGGREGATES

Starting with a single monomer, a TB aggregate is created by randomly attaching a new monomer to the already existing one(s) until the desired number of monomers N is reached (Fig. 2). The study by Girotto *et al.* [8] indicated that although a large fraction (48%) of the TB aggregates consisted of eight to 10 monomers, a significant (52%) fraction of particles were composed of 11 or more monomers, with a minor 3% of the TB aggregates having between 80 and 110 monomers. To cover a representative range of N , we consider the following numbers of monomers per aggregate: $N = 4, 6, 8, 10, 20, 30, 40, 50, 60, 70, 80, 90, 100, 110$, and 120. We assume that the polydispersion of monomer radii r in a TB aggregate is described by the standard log normal distribution [20,21],

$$n(r) = \text{constant} \times \frac{1}{r} \exp \left[-\frac{(\ln r - \ln r_g)^2}{2 \ln^2 \sigma_g} \right], \quad (1)$$

where r_g is the geometric mean radius and σ_g is the geometric mean standard deviation. In this study we use two geometric mean radius values, $r_g = 75$ and 100 nm, the corresponding geometric mean standard deviation being fixed so that $\ln^2 \sigma_g = 0.05$. The values $r_g = 75$ nm and $\ln^2 \sigma_g = 0.05$ are consistent with the measurements in [8], while $r_g = 100$ nm is close to the upper limit of observed values in [6].

Note that possible geometrical configurations of the same group of monomers constituting a TB aggregate are virtually infinite. To account for the variation in the radiative properties of TBs caused by this morphological diversity, for each N value ($N = 4, 6, \dots, 120$) listed above, we arrange the monomers randomly and thereby generate 10 different aggregates, each having its own geometrical configuration. The majority of the results presented in this study are ensemble averages over these 10 geometrical realizations of aggregates consisting of the same monomers and are calculated following Eqs. (5)–(9) of Liu and Mishchenko [22]. We have verified that the averaged values thus calculated can be satisfactorily used to describe the radiative

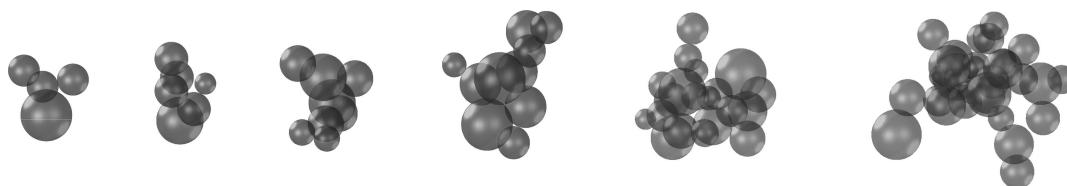


Fig. 2. Examples of tar-ball aggregates consisting of $N = 4, 6, 8, 10, 20$, and 30 (from left to right) primary spherules parameterized according to Eq. (1) with $r_g = 75$ nm and $\ln^2 \sigma_g = 0.05$.

Table 1. Refractive Indices of Tar Balls Used in This Study

Reference	$\lambda = 355$ nm	$\lambda = 532$ nm	$\lambda = 1064$ nm
[24]	$1.572 + i0.334$	$1.668 + i0.278$	$1.778 + i0.189$
[28]	$1.541 + i0.022$	$1.532 + i0.003$	$1.530 + i0.002$

properties of the entire ensemble of tar ball aggregates composed of the same group of monomers.

We have computed light scattering and absorption by TB aggregate aerosols at three wavelengths ($\lambda = 355$, 532, and 1064 nm) representing the spectral channels of the NASA Langley airborne High Spectral Resolution Lidar 2 (HSRL2) [23]. BrC materials absorb primarily blue and ultraviolet light while black carbon absorbs broadly across the visible spectrum.

The published refractive indices of BrC aerosols vary substantially in terms of absorptivity and its spectral dependence [2,11,24–27]. We used the two extreme cases representing the most [24] and the least [28] absorptive BrC. The corresponding refractive indices are listed in Table 1.

3. ELECTROMAGNETIC SCATTERING

In this study, we use the STMM to calculate ensemble-averaged absorption and scattering characteristics of TB aggregates. The STMM is a first-principles scattering methodology rendering direct computer solutions of the macroscopic Maxwell equations [17–19]. For the particle morphologies studied in this paper, the STMM is by far the most efficient numerically exact technique.

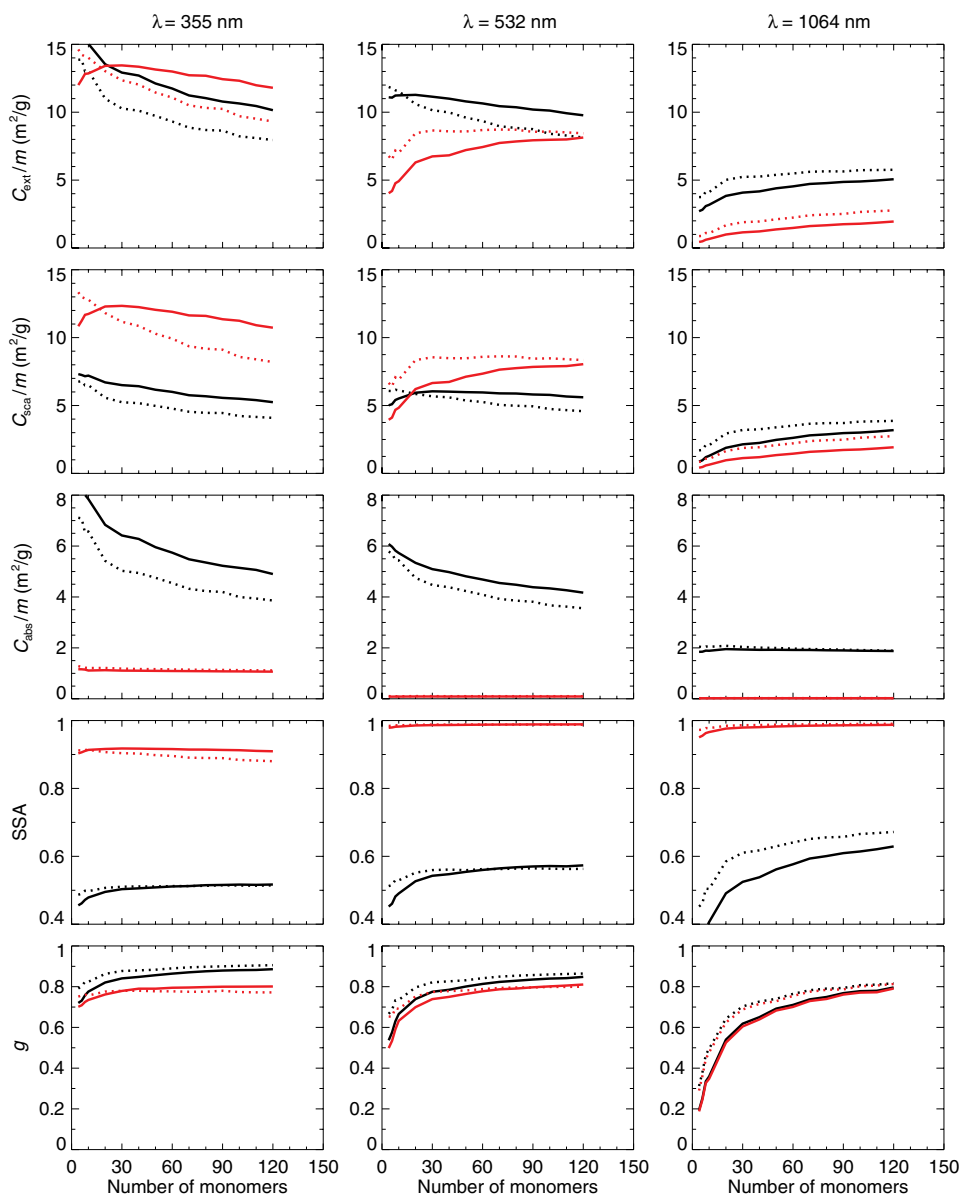


Fig. 3. Integral radiative characteristics of different TB aggregates at three wavelengths. The black and red curves depict the STMM results computed for the refractive indices from [24] and [28], respectively. The solid and dotted curves show the results for $r_g = 75$ and 100 nm, respectively.

Consistent with [29], we assume that all TB aggregates are randomly oriented and form a statistically isotropic and mirror-symmetric ensemble. The key single-scattering characteristics we focus on include the ensemble-averaged extinction, C_{ext} , scattering, C_{sca} , and absorption, C_{abs} , cross sections per particle, the single-scattering albedo (SSA), and the asymmetry parameter g , as well as the elements of the normalized 4×4 Stokes scattering matrix. The latter has the well-known block-diagonal structure [21,30],

$$\tilde{\mathbf{F}}(\Theta) = \begin{bmatrix} a_1(\Theta) & b_1(\Theta) & 0 & 0 \\ b_1(\Theta) & a_2(\Theta) & 0 & 0 \\ 0 & 0 & a_3(\Theta) & b_2(\Theta) \\ 0 & 0 & -b_2(\Theta) & a_4(\Theta) \end{bmatrix}, \quad (2)$$

where $\Theta \in [0, \pi]$ is the scattering angle. The (1,1) element of the scattering matrix, $a_1(\Theta)$, is the conventional phase function,

which is normalized according to

$$\frac{1}{2} \int_0^\pi d\Theta \sin \Theta a_1(\Theta) = 1. \quad (3)$$

It describes the angular distribution of the scattered intensity in the case of unpolarized incident light. The conventional lidar linear depolarization ratio (LDR) is defined by

$$\delta_L = \frac{a_1(180^\circ) - a_2(180^\circ)}{a_1(180^\circ) + a_2(180^\circ)}, \quad (4)$$

while the degree of linear polarization of the scattered light for the case of unpolarized incident light is given by $-b_1(\Theta)/a_1(\Theta)$.

For completeness of discussion, we compare the T -matrix results calculated for a TB aggregate with the corresponding Lorenz–Mie results, based on the assumption that (i) each monomer in the aggregate is externally mixed with and widely separated from the other primary particles [see Fig. 1(a)], or

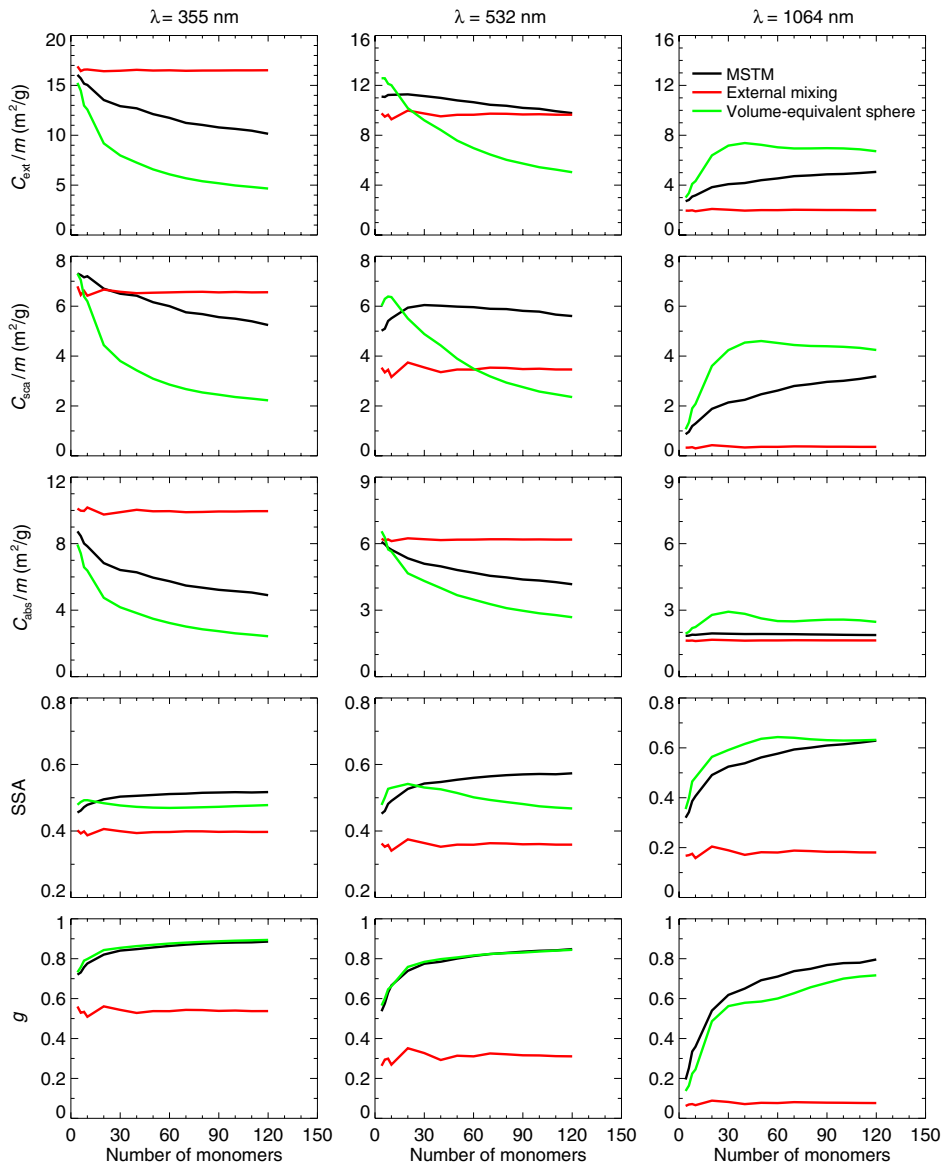


Fig. 4. Ensemble-averaged integral radiative characteristics as functions of the number of monomers per TB aggregate for $r_g = 75$ nm.

(ii) the TB aggregate is replaced by a single volume-equivalent sphere. The external-mixing approximation and the volume-equivalent sphere model are frequently used in climate studies to represent the scattering and absorption properties of BrC and other morphologically complex aerosols. Our numerically exact STMM results can thus be used to quantize the errors of these simplistic approaches.

4. RESULTS

In Fig. 3 we plot the integral radiative characteristics; viz., the ensemble-averaged mass specific extinction, C_{ext}/m , scattering, C_{sca}/m , and absorption, C_{abs}/m , cross sections, the SSA, and the asymmetry parameter, where m is the cumulative mass of a TB aggregate. In other words, the mass specific cross sections are defined as the per unit mass of the BrC material. The effective density of primary BrC particles varies from about 0.85 to 1.19 g/cm³ [31]. However, for the sake of simplicity, we have adopted a constant value of 1 g/cm³.

Obviously, spectrally dependent refractive indices and sizes are two important parameters strongly affecting the integral radiative properties of TB aggregates. Indeed, changing the refractive index from $1.572 + i0.334$ to $1.541 + i0.022$ (see Table 1) can approximately double the mass specific scattering cross section at 355 nm. However, at a longer wavelength of 1064 nm, TB aggregates with the refractive index from [24]

scatter twice as much light as their counterparts with the refractive index from [28]. Absorption is negligibly weak at visible and infrared wavelengths in the case of the least absorptive BrC. On the other hand, in the case of the most absorptive BrC, the C_{abs}/m values at 355 nm and 532 nm are large enough to be comparable to the absorption by soot aerosols (see [32] and references therein). Overall, for the particular cases analyzed in this study, smaller TB aggregates (with fewer primary particles) composed of smaller monomers are more efficient light absorbers at 355 and 532 nm. This may be caused by a shielding effect of the outer layer of monomers that blocks light from penetrating deeply inside the larger TB aggregates with more monomers.

The SSA has a particular climatological significance since its critical value at which the aerosol impact on global mean surface temperature changes from cooling to heating occurs in a relatively narrow range, with $\text{SSA} \approx 0.86$ in climate simulations with fixed clouds and $\text{SSA} \approx 0.91$ in the case of interactive clouds [33]. Due to the large spread in the reported imaginary part of the refractive indices of BrC aerosols, their climate impact can range from strong to weak warming and even cooling, as evidenced by the dramatic values of the differences in the SSAs.

Compared to the particle sizes, particle refractive indices have a rather small effect on the asymmetry parameter, particularly at

Table 2. C_{abs} , SSA, and g of Tar Ball Aggregates With Two Different Geometrical Mean Radii r_g of Monomers for Two Sets of Refractive Indices at Three Wavelengths

λ (nm)	Ratio	$r_g = 75$ nm				$r_g = 100$ nm				
		[24] ^c		[28] ^d		[24]		[28]		
		v_{min}^e	v_{max}^f	v_{min}	v_{max}	v_{min}	v_{max}	v_{min}	v_{max}	
C_{abs}	355	Ext/cluster ^a	1.156	2.031	0.976	1.043	1.184	2.244	1.016	1.126
		VES/cluster ^b	0.496	0.909	1.067	1.269	0.447	0.876	0.921	1.131
	532	Ext/cluster	1.023	1.483	0.867	0.912	1.075	1.798	0.933	0.968
		VES/cluster	0.643	1.079	1.236	1.678	0.535	0.968	1.122	1.586
	1064	Ext/cluster	0.844	0.883	0.813	0.912	0.876	0.968	0.823	0.926
		VES/cluster	1.051	1.513	1.044	1.753	1.068	1.345	1.080	1.783
SSA	355	Ext/cluster	0.768	0.883	0.959	0.970	0.876	0.930	0.986	1.028
		VES/cluster	0.916	1.056	0.742	1.012	0.922	1.012	0.760	1.005
	532	Ext/cluster	0.626	0.802	0.979	0.989	0.784	0.894	0.990	0.996
		VES/cluster	0.816	1.094	0.992	1.004	0.819	1.037	0.968	1.003
	1064	Ext/cluster	0.287	0.523	0.911	0.937	0.459	0.758	0.958	0.983
		VES/cluster	1.005	1.204	1.004	1.012	0.867	1.128	1.001	1.008
g	355	Ext/cluster	0.607	0.778	0.675	0.805	0.739	0.863	0.818	0.903
		VES/cluster	1.009	1.043	0.690	1.013	1.002	1.021	0.707	1.065
	532	Ext/cluster	0.366	0.512	0.345	0.479	0.555	0.764	0.586	0.823
		VES/cluster	0.994	1.053	0.864	1.132	1.004	1.035	0.645	1.039
	1064	Ext/cluster	0.096	0.320	0.085	0.293	0.165	0.503	0.142	0.461
		VES/cluster	0.651	0.911	0.569	0.906	0.833	0.966	0.700	0.996

^a Ratios of the optical properties calculated for the external mixtures (Ext) to those of the corresponding TB aggregates.

^b Ratios of the optical properties calculated for the volume-equivalent spheres (VES) to those of the corresponding TB aggregates.

^c Spectral refractive indices of TBs are from [24], representing the most absorptive BrC material reported.

^d Spectral refractive indices of TBs are from [28], representing the least absorptive BrC material reported.

^e Minimum value among the ratios Ext/cluster or VES/cluster calculated for 15 sets of TB-clusters with the number of monomers $N = 4, 6, \dots, 120$ for a given wavelength, r_g , and refractive index.

^f Maximum value among the ratios Ext/cluster or VES/cluster calculated for 15 sets of TB-clusters with the number of monomers $N = 4, 6, \dots, 120$ for a given wavelength, r_g , and refractive index.

longer wavelengths. It is not surprising since g is mostly defined by the cluster size and morphology.

Figure 4 compares the numerically exact STMM results and those obtained using the external mixing approximation and the volume-equivalent-sphere model using the refractive indices from [24]. The differences between the exact and approximate results are obviously quite substantial. It is well known that for soot fractal aggregates composed of strongly absorptive Rayleigh-sized spherules, aggregation can result in a significant enhancement of absorption relative to that computed for idealized spherically shaped aerosol external mixtures using the Lorenz–Mie theory (e.g., [14,22,34–36]). However, possibly due to their large monomer sizes and mutual shadowing, TB aggregates are less effective in absorbing light than their external-mixture counterparts, in which each tar ball is fully exposed to the incident radiation. The differences between the two decrease with increasing wavelength. At a

longer wavelength (i.e., 1064 nm), the former become stronger light absorbers again, much the same as what we have observed for soot fractals. The most profound effects of aggregation are on the SSA and asymmetry parameter, in which case the aggregates can have SSA and g values larger than those of the “equivalent” external mixtures by about 0.21 and 0.54, respectively, at 532 nm. This is quite consistent with the conclusions reached by Bhandari *et al.* [6]. Significant as they are, these enhancements in the SSA and asymmetry parameter caused by aggregation are still less prominent than those for soot aggregates, wherein the enhancement ratios can sometimes exceed two orders of magnitude [14].

The integral radiative characteristics of the TB clusters are also significantly different from those of the volume-equivalent homogeneous spheres. Overall, the clusters have larger mass specific scattering and absorption cross sections and SSAs at the two shorter wavelengths, while the opposite tends to be true

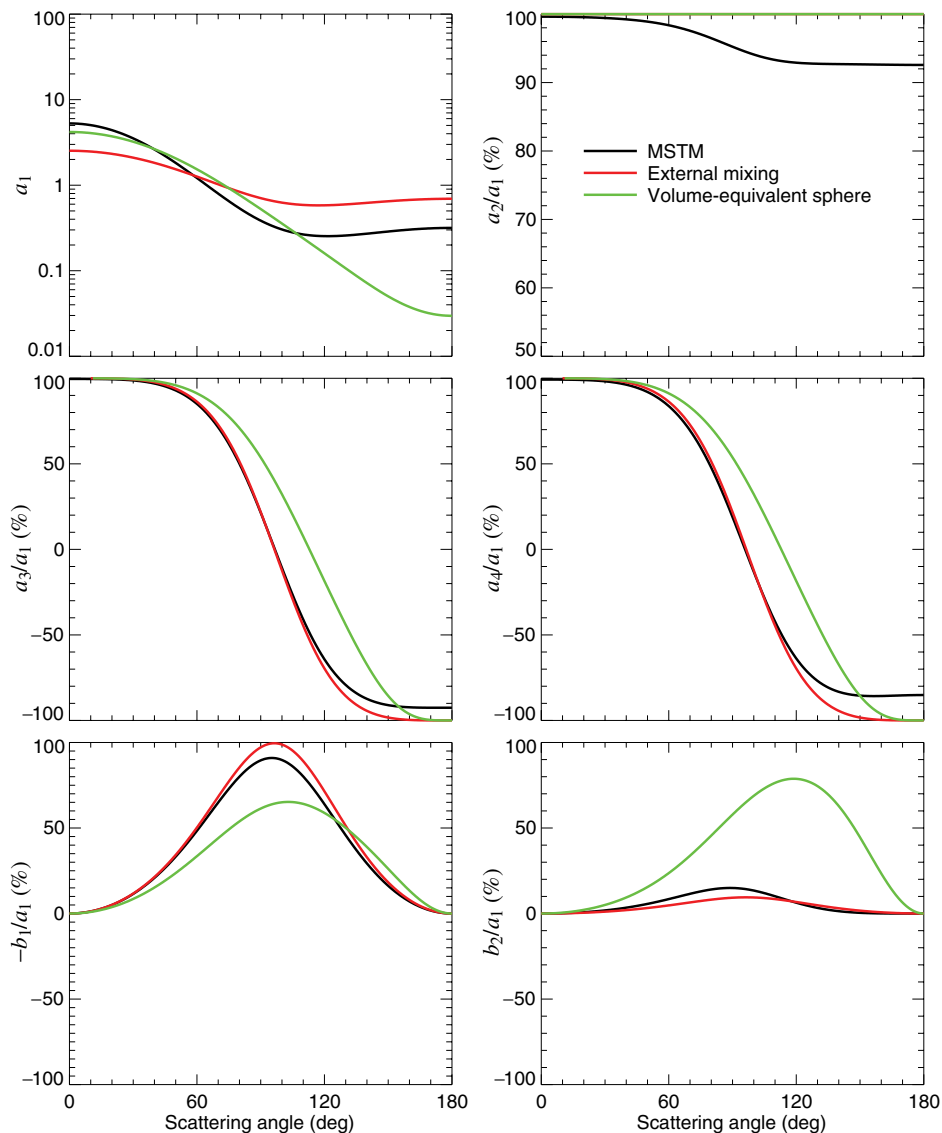


Fig. 5. Black curves: ensemble-averaged Stokes scattering matrix elements for a TB aggregate composed of four monomers at 532 nm using the BrC refractive index from [24]. The red and green curves show the results calculated for the “equivalent” external mixture of the same four monomers and the single volume-equivalent sphere.

at 1064 nm. Possibly due to the already large overall size of the particles, the differences in the asymmetry parameter between the aggregates and the corresponding equal-volume spheres are rather small.

The effect of aggregation on the integral radiative characteristics of TB aggregates depends on several factors such as the refractive index, the number of monomers and their sizes, and the wavelength, as evidenced by Table 2. It summarizes the ranges of the ratios of three important optical parameters of 15 sets of TB aggregates composed of different numbers of monomers ($N = 4, 6, \dots, 120$) to those calculated for the corresponding external mixtures and volume-equivalent spheres. The table contains results calculated for two different geometrical mean monomer radii and two sets of spectral refractive indices at the three HSRL2 wavelengths. Obviously the patterns displayed in Fig. 4 (corresponding to the values in columns 4 and 5) are not exactly the same for the case of the least absorptive BrC (columns 6 and 7), where the SSAs of the TB aggregates are only slightly increased compared to their external mixture counterparts, and aggregation results in enhanced absorption at both wavelengths 532 and 1064 nm. The patterns displayed in columns 4 and 5 are also different from columns 8 and 9 when $r_g = 100$ nm. This implies the pivotal role that the particle size,

morphology, and refractive index play in defining the radiative properties of TB aggregates.

Figure 5 compares the ensemble averaged scattering matrix elements averaged over 10 TB aggregate realizations with those computed for the corresponding external mixture and the homogeneous equal-volume sphere. The wavelength is 532 nm, and the corresponding refractive index is taken from [24]. The number of TBs in the aggregate is four with $r_g = 75$ nm. Clearly, the independent-spherule model provides a poor representation of the cluster phase function, whereas the performance of the equal-volume-sphere model is inadequate with respect to all scattering matrix elements. This demonstrates once again the inadequacy of using the Lorenz–Mie theory to simulate light scattering by aggregated aerosols. Even for such a small tar ball aggregate, which contains of only four monomers, the overall single scattering characteristics obviously deviate from those of a sphere, as evidenced by the non-unity value of the ratio $a_2(180^\circ)/a_1(180^\circ)$ and the deviation of the ratios $a_3(180^\circ)/a_1(180^\circ)$ and $a_4(180^\circ)/a_1(180^\circ)$ from -1 . At the exact forward-scattering direction, electromagnetic interactions between the monomers result in a rather significant enhancement of the aggregate phase function. Due to the relatively large monomer sizes and the scattering interactions among them, the

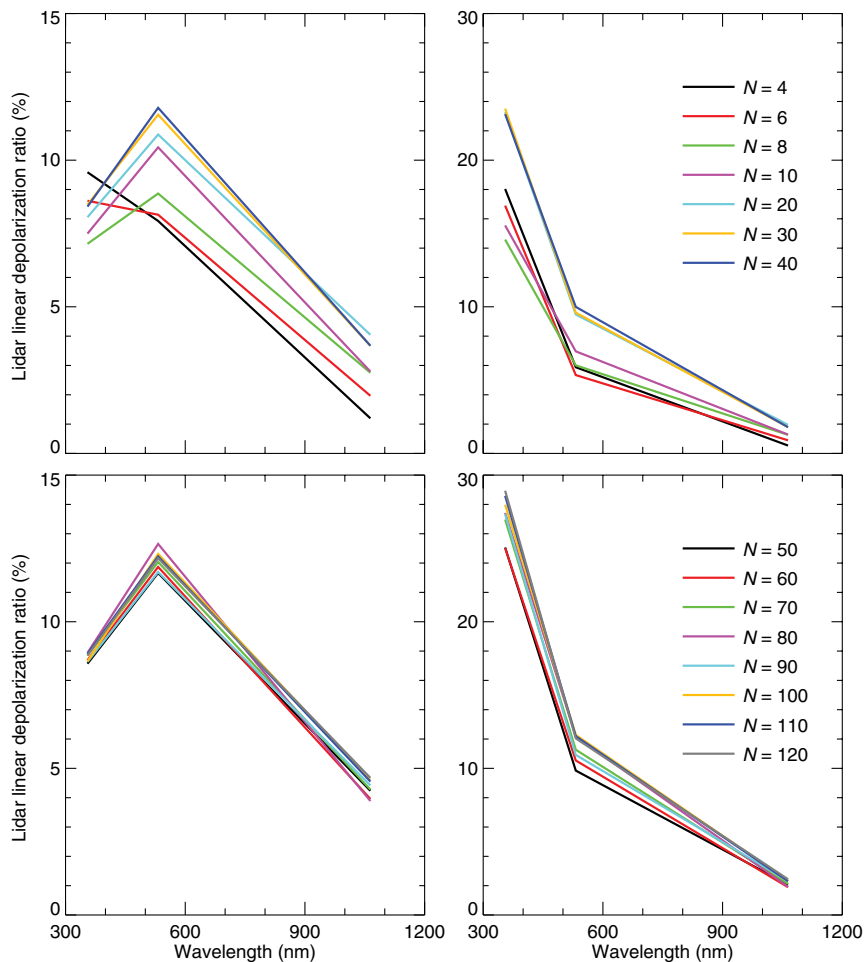


Fig. 6. Wavelength-dependent backscattering linear depolarization ratios for TB aggregates with the number of monomers ranging from 4, 6, 8, \dots , to 40 (top row) and from 50 to 120 calculated using the refractive indices from [24] (left-hand column) and from [28] (right-hand column). The geometrical mean radius of the component monomers is fixed at 100 nm.

degree of linear polarization of scattered light for unpolarized incident light, $-b_1(\Theta)/a_1(\Theta)$ starts deviating from the typical traits of Rayleigh scatterers whose linear polarization ratio is zero at the exact forward-scattering and back-scattering directions, and reaches a nearly 100% maximum at $\Theta \approx 90^\circ$ while the $b_2(\Theta)/a_1(\Theta)$ values are very close to zero. As the number of monomers grows, the overall single-scattering characteristics computed for the homogeneous equal-volume sphere progressively further deviate from those of the ensemble averaged scattering matrix elements of TB aggregates.

Figure 6 depicts wavelength-dependent LDRs for TB aggregates with the number of monomers $N = 4, 6, \dots, 120$ calculated using the refractive indices from [24,28]. The geometrical mean monomer radius in each of the aggregates is $r_g = 100$ nm. Obviously the spectrally dependent LDRs are very sensitive to the change of particle refractive indices. For very absorptive BrC (left-hand column), the LDRs caused by particle nonsphericity are rather high. The LDRs are generally lower at 355 nm than at 532 nm, and decrease significantly toward 1064 nm. In contrast, the LDRs at 355 nm for the least absorptive BrC material (right-hand column) are even higher and gradually increase with the overall particle dimension up to about 29%, with a strong negative spectral slope. When $N = 30, 40, 50,$ and 60 , the calculated depolarization spectrum is within the range observed for an aged wildfire smoke

plume by Burton *et al.* [23] ($\delta_L = 0.203 \pm 0.053$ at 355 nm, 0.093 ± 0.026 at 532 nm, and 0.018 ± 0.009 at 1064 nm). Kahnert [37], Burton *et al.* [23], and especially Mishchenko *et al.* [38] and Liu and Mishchenko [15], have demonstrated that specific complex morphologies of soot-containing aerosols can reproduce LDRs with such exceptionally high values and unusual spectral dependence. Our new study shows that not only aged soot particles, but also BrC aerosols (i.e., TB aggregates), which are also abundant in smoke plumes, can reproduce the same depolarization spectrum.

To parallel Fig. 6, Fig. 7 shows the sensitivity of lidar LDRs to particle monomer sizes when everything is the same as in Fig. 6 except that the geometrical mean monomer radius in each aggregate is now 75 nm rather than 100 nm. It is immediately clear that reducing monomer sizes decreases the LDRs significantly and causes them to decrease with increasing wavelength irrespective of the choice of refractive index. When the geometrical mean monomer radius is reduced from 100 nm to 75 nm, the TB clusters are no longer capable of generating the exceptionally high spectral LDRs that match the lidar observations in [23]. Interestingly, the LDRs at 355 nm in the right-hand column are generally higher than their “strongly absorptive” counterparts, while the opposite is true at 532 nm. Also of note is that the TB aggregates with as few as $N = 4$ monomers cause the largest (or near-largest) LDRs at the ultraviolet wavelength. Our study

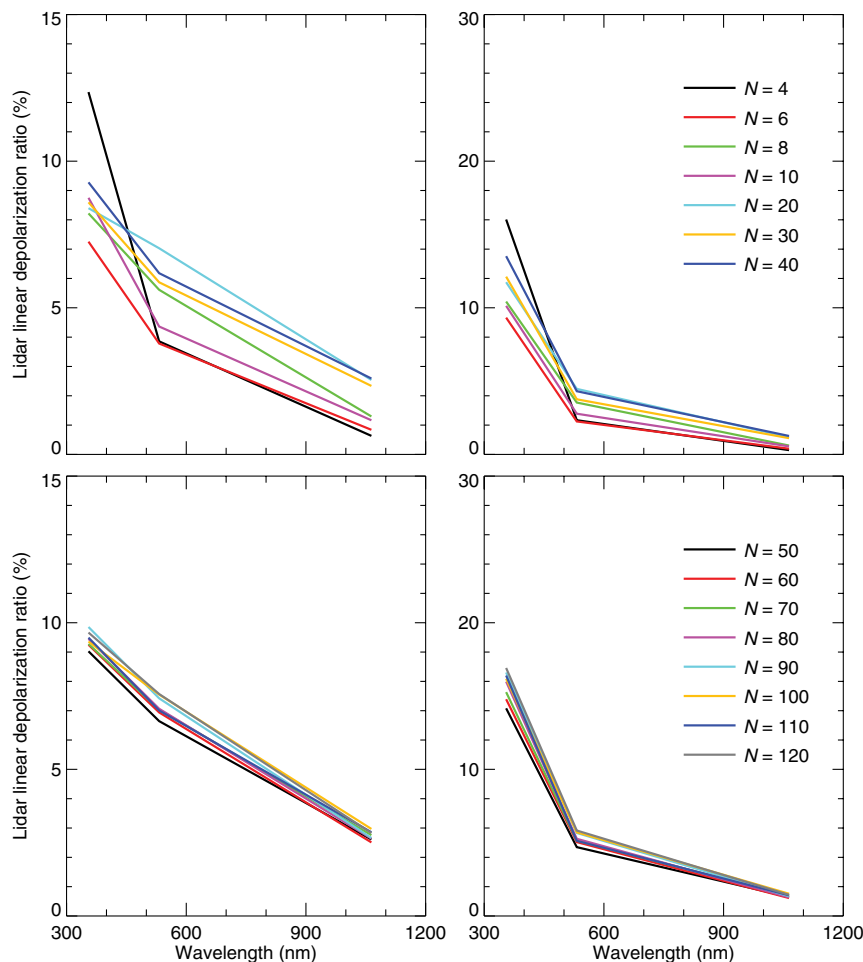


Fig. 7. As in Fig. 6, except that the geometrical mean radius of the monomers in each aggregate is 75 nm.

emphasizes again the potential of using depolarization measurements at multiple wavelengths to identify and characterize smoke particles.

5. CONCLUSIONS

We have used the STMM to compute the scattering matrix elements and optical cross sections for a variety of TB aggregates, each of which is composed of a number of monomers whose sizes follow a lognormal distribution. The errors caused by employing the external-mixing approximation and the model wherein a large homogeneous sphere is used to represent a cluster of the same total volume are quite significant, both in the integral photometric characteristics and in the Stokes scattering matrix elements. Aggregation of individual TBs into a cluster can either enhance or weaken absorption, depending on the wavelength, the monomer size, and how absorptive the BrC material is. For example, for the case of strongly absorptive BrC, aggregation results in enhanced absorption only at 1064 nm, while at the two shorter wavelengths, 355 and 532 nm, TB aggregates become less effective absorbers compared to the corresponding external mixtures. For the least absorptive BrC material, aggregation induces enhanced absorption at wavelengths of 532 and 1064 nm. The effect of aggregation is always to increase the SSA and asymmetry parameter, sometimes by more than a factor of 10. The significant scattering-matrix differences between the aggregates, the “equivalent” external mixtures, and the volume-equivalent sphere model demonstrate the failure of the conventional Lorenz–Mie theory to represent the scattering properties of morphologically complex BrC aerosols. In the future, we plan to investigate if using an equal-volume-spheroidal model would yield a better match to the radiative properties calculated for the morphologically complex carbonaceous aerosols using the STMM.

Although some of our TB aggregate models are able to reproduce the spectrum of backscattering LDRs observed by Burton *et al.* [23], the theoretical LDRs at 532 nm are not high enough to match the newer lidar measurements by Haarig *et al.* [39] and Hu *et al.* [40]. Both studies have reported very high LDRs at 355 nm and 532 nm, with very weak spectral dependence between the two wavelengths. They have concluded that such wavelength-dependent LDRs were caused by dry irregularly shaped soot. However, based on our study and some previous research, they are likely due to the combined effect of soot, BrC aerosols like TB aggregates, and some fine dust. Moreover, in addition to backscattering LDRs, spectrally resolved lidar ratios are also measured by HSRL2. We plan to examine the combined use of lidar ratios and LDRs for a better and more accurate characterization of carbonaceous aerosols.

Funding. National Aeronautics and Space Administration.

Acknowledgment. We thank two anonymous reviewers for useful comments and suggestions.

REFERENCES

1. M. Pósfai, A. Gelencsér, R. Simonics, K. Arató, J. Li, P. V. Hobbs, and P. R. Buseck, “Atmospheric tar balls: particles from biomass and bio-fuel burning,” *J. Geophys. Res.* **109**, D06213 (2004).
2. J. L. Hand, W. C. Malm, A. Laskin, D. Day, T. Lee, C. Wang, C. Carrico, J. Carrillo, J. P. Cowin, J. Collett, and M. J. Iedema, “Optical, physical, and chemical properties of tar balls observed during the Yosemite Aerosol Characterization Study,” *J. Geophys. Res.* **110**, D21210 (2005).
3. K. Adachi and P. R. Buseck, “Atmospheric tar balls from biomass burning in Mexico,” *J. Geophys. Res.* **116**, D05204 (2011).
4. J. Chen, C. Li, Z. Ristovski, A. Milic, Y. Gu, M. S. Islam, S. Wang, J. Hao, H. Zhang, C. He, H. Guo, H. Fu, B. Miljevic, L. Morawska, P. Thai, Y. F. Lam, G. Pereira, A. Ding, X. Huang, and U. C. Dumka, “A review of biomass burning: emissions and impacts on air quality, health and climate in China,” *Sci. Total Environ.* **579**, 1000–1034 (2017).
5. R. K. Chakrabarty, M. Gyawali, R. L. N. Yatavelli, A. Pandey, A. C. Watts, J. Knue, L. W. A. Chen, R. R. Pattison, A. Tsibert, V. Samburova, and H. Moosmüller, “Brown carbon aerosols from burning of boreal peatlands: microphysical properties, emission factors, and implications for direct radiative forcing,” *Atmos. Chem. Phys.* **16**, 3033–3040 (2016).
6. J. Bhandari, S. China, G. Giroto, B. Scarnato, K. Gorkowski, A. Aiken, M. Dubey, and C. Mazzoleni, “Optical properties and radiative forcing of fractal-like tar ball aggregates from biomass burning,” *J. Quant. Spectrosc. Radiat. Transfer* **230**, 65–74 (2019).
7. C. Li, Q. He, J. Schade, J. Passig, R. Zimmermann, D. Meidan, A. Laskin, and Y. Rudich, “Dynamic changes in optical and chemical properties of tar ball aerosols by atmospheric photochemical aging,” *Atmos. Chem. Phys.* **19**, 139–163 (2019).
8. G. Giroto, S. China, J. Bhandari, K. Gorkowski, B. V. Scarnato, T. Capek, A. Marinoni, D. P. Veghte, G. Kulkarni, A. C. Aiken, M. Dubey, and C. Mazzoleni, “Fractal-like tar ball aggregates from wildfire smoke,” *Environ. Sci. Technol. Lett.* **5**, 360–365 (2018).
9. K. Deboudt, P. Flament, M. Choel, A. Gloter, S. Sobanska, and C. Colliex, “Mixing state of aerosols and direct observation of carbonaceous and marine coatings on African dust by individual particle analysis,” *J. Geophys. Res.* **115**, D24207 (2010).
10. A. Tóth, A. Hoffer, I. Nyirő-Kósa, M. Pósfai, and A. Gelencsér, “Atmospheric tar balls: aged primary droplets from biomass burning?” *Atmos. Chem. Phys.* **14**, 6669–6675 (2014).
11. A. J. Sedlacek, III, P. R. Buseck, K. Adachi, T. B. Onasch, S. R. Springston, and L. Kleinman, “Formation and evolution of tar balls from northwestern US wildfires,” *Atmos. Chem. Phys.* **18**, 11289–11301 (2018).
12. J. Li, M. Pósfai, P. V. Hobbs, and P. R. Buseck, “Individual aerosol particles from biomass burning in southern Africa: 2. Compositions and aging of inorganic particles,” *J. Geophys. Res.* **108**, 8484 (2003).
13. S. China, N. Salvadori, and C. Mazzoleni, “Effect of traffic and driving characteristics on morphology of atmospheric soot particles at free-way on-ramps,” *Environ. Sci. Technol.* **48**, 3128–3135 (2014).
14. L. Liu, M. I. Mishchenko, and W. P. Arnott, “A study of radiative properties of fractal soot aggregates using the superposition T-matrix method,” *J. Quant. Spectrosc. Radiat. Transfer* **109**, 2656–2663 (2008).
15. L. Liu and M. I. Mishchenko, “Scattering and radiative properties of morphologically complex carbonaceous aerosols: a systematic modeling study,” *Remote Sens.* **10**, 1634 (2018).
16. C. Liu, X. Xu, Y. Yin, M. Schnaiter, and Y. L. Yung, “Black carbon aggregates: a database for optical properties,” *J. Quant. Spectrosc. Radiat. Transfer* **222–223**, 170–179 (2019).
17. D. W. Mackowski and M. I. Mishchenko, “Calculation of the T matrix and the scattering matrix for ensembles of spheres,” *J. Opt. Soc. Am. A* **13**, 2266–2278 (1996).
18. D. W. Mackowski and M. I. Mishchenko, “A multiple sphere T-matrix Fortran code for use on parallel computer clusters,” *J. Quant. Spectrosc. Radiat. Transfer* **112**, 2182–2192 (2011).
19. D. W. Mackowski, “A general superposition solution for electromagnetic scattering by multiple spherical domains of optically active media,” *J. Quant. Spectrosc. Radiat. Transfer* **133**, 264–270 (2014).

20. J. E. Hansen and L. D. Travis, "Light scattering in planetary atmospheres," *Space Sci. Rev.* **16**, 527–610 (1974).
21. M. I. Mishchenko, L. D. Travis, and A. A. Lacis, *Scattering, Absorption, and Emission of Light by Small Particles* (Cambridge University, 2002).
22. L. Liu and M. I. Mishchenko, "Scattering and radiative properties of complex soot and soot-containing aggregate particles," *J. Quant. Spectrosc. Radiat. Transfer* **106**, 262–273 (2007).
23. S. P. Burton, J. W. Hair, M. Kahnert, R. A. Ferrare, C. A. Hostetler, A. L. Cook, D. B. Harper, T. A. Berkoff, S. T. Seaman, J. E. Collins, M. A. Fenn, and R. R. Rogers, "Observations of the spectral dependence of linear particle depolarization ratio of aerosols using NASA Langley airborne high spectral resolution lidar," *Atmos. Chem. Phys.* **15**, 13453–13473 (2015).
24. D. T. Alexander, P. A. Crozier, and J. R. Anderson, "Brown carbon spheres in East Asian outflow and their optical properties," *Science* **321**, 833–836 (2008).
25. R. Chakrabarty, H. Moosmüller, L. W. Chen, K. Lewis, W. Arnott, C. Mazzoleni, M. Dubey, C. Wold, W. Hao, and S. Kreidenweis, "Brown carbon in tar balls from smoldering biomass combustion," *Atmos. Chem. Phys.* **10**, 6363–6370 (2010).
26. A. Hoffer, Á. Tóth, I. Nyirő-Kósa, M. Pósfai, and A. Gelencsér, "Light absorption properties of laboratory-generated tar ball particles," *Atmos. Chem. Phys.* **16**, 239–246 (2016).
27. A. Hoffer, Á. Tóth, M. Pósfai, C. E. Chung, and A. Gelencsér, "Brown carbon absorption in the red and near-infrared spectral region," *Atmos. Meas. Tech.* **10**, 2353–2359 (2017).
28. B. J. Sumlin, Y. W. Heinson, N. Shetty, A. Pandey, R. S. Pattison, S. Baker, W. M. Hao, and R. K. Chakrabarty, "UV-Vis-IR spectral complex refractive indices and optical properties of brown carbon aerosol from biomass burning," *J. Quant. Spectrosc. Radiat. Transfer* **206**, 392–398 (2018).
29. M. I. Mishchenko and M. A. Yurkin, "On the concept of random orientation in far-field electromagnetic scattering by nonspherical particles," *Opt. Lett.* **42**, 494–497 (2017).
30. M. I. Mishchenko, *Electromagnetic Scattering by Particles and Particle Groups: An Introduction* (Cambridge University, 2014).
31. B. J. Sumlin, C. R. Oxford, B. Seo, R. R. Pattison, B. J. Williams, and R. K. Chakrabarty, "Density and homogeneous internal composition of primary brown carbon aerosol," *Environ. Sci. Technol.* **52**, 3982–3989 (2018).
32. S. Nordmann, W. Birmili, K. Weinhold, K. Müller, G. Spindler, and A. Wiedensohler, "Measurements of the mass absorption cross section of atmospheric soot particles using Raman spectroscopy," *J. Geophys. Res. Atmos.* **118**, 12075–12085 (2013).
33. J. Hansen, M. Sato, and R. Ruedy, "Radiative forcing and climate response," *J. Geophys. Res.* **102**, 6831–6864 (1997).
34. L. Liu and M. I. Mishchenko, "Effects of aggregation on scattering and radiative properties of soot aerosols," *J. Geophys. Res.* **110**, D11211 (2005).
35. M. Kahnert and A. Devasthale, "Black carbon fractal morphology and short-wave radiative impact: a modeling study," *Atmos. Chem. Phys.* **11**, 11745–11759 (2011).
36. Y. Wu, X. Gu, T. Cheng, D. Xie, T. Yu, H. Chen, and J. Guo, "The single scattering properties of the aerosol particles as aggregated spheres," *J. Quant. Spectrosc. Radiat. Transfer* **113**, 1454–1466 (2012).
37. M. Kahnert, "Optical properties of black carbon aerosols encapsulated in a shell of sulfate: comparison of the closed cell model with a coated aggregate model," *Opt. Express* **25**, 24579–24593 (2017).
38. M. I. Mishchenko, J. M. Dlugach, and L. Liu, "Linear depolarization of lidar returns by aged smoke particles," *Appl. Opt.* **55**, 9968–9973 (2016).
39. M. Haarig, A. Ansmann, H. Baars, C. Jimenez, I. Veselovskii, R. Engelmann, and D. Althausen, "Depolarization and lidar ratios at 355, 532, and 1064 nm and microphysical properties of aged tropospheric and stratospheric Canadian wildfire smoke," *Atmos. Chem. Phys.* **18**, 11847–11861 (2018).
40. Q. Hu, P. Goloub, I. Veselovskii, J.-A. Bravo-Aranda, I. Popovici, T. Podvin, M. Haeffelin, A. Lopatin, C. Pietras, X. Huang, B. Torres, and X. Chen, "A study of long-range transported smoke aerosols in the upper troposphere/lower stratosphere," *Atmos. Chem. Phys.* **19**, 1173–1193 (2019).